Dyes and Pigments 189 (2021) 109251

Contents lists available at ScienceDirect

Dyes and Pigments

journal homepage: http://www.elsevier.com/locate/dyepig

Synthesis and characterization of benzotriazolyl acrylonitrile analogs-based donor-acceptor molecules: Optical properties, *in vitro* cytotoxicity, and cellular imaging

Eugenio Hernández-Fernández [a,*], Ana Sofia Ortega-Villarreal [a], Ma. Concepción García-López [b], Rodrigo Chan-Navarro [a], Samuel Garrard [c], Gabriel A. Valdivia-Berroeta [c], Stacey J. Smith [c], Kenneth A. Christensen [c], David J. Michaelis [c,**]

[a] Universidad Autónoma de Nuevo León, Facultad de Ciencias Químicas, Pedro de Alba s/n, Ciudad Universitaria, 66455, San Nicolás de Los Garza, Nuevo León, Mexico
[b] CONACYT-Universidad Autónoma de Nuevo León, Facultad de Ciencias Químicas, Pedro de Alba s/n, Ciudad Universitaria, 66455, San Nicolás de Los Garza, Nuevo León, Mexico
[c] Department of Chemistry and Biochemistry, Brigham Young University, 84602, Provo, UT, United States

ARTICLE INFO

Keywords:
Lysosome/endosome staining
Cellular imaging
Benzotriazole
Acrylonitrile analogs
Confocal microscopy

ABSTRACT

A series of eight new (*E*)-benzotriazolyl acrylonitrile derivatives were synthesized under reflux conditions *via* Knoevenagel condensation between acetonitrile analogs and a short series of aromatic aldehydes. X-ray diffraction analysis for one of the compounds was performed to determine the (*E*)-geometry of its double bond. The photoluminescent properties of all compounds in solution were also evaluated. These compounds exhibit strong blue, green and yellow emission under ultraviolet light excitation with fluorescence quantum yield in the 0.08–0.58% range. To determine the suitability of these compounds for use in cell-based analysis, cytotoxicity assays were performed on a representative molecule using a common mammalian cell line (HEK 293T cells) at different concentrations. The results showed limited toxicity (72 ± 16% viability) at the highest concentration tested (50 μM). Finally, confocal microscopy demonstrated that our compound was internalized into cells and localized to endosomes and/or lysosomes in a similar fashion to Dextran–Cascade Blue (DCB).

1. Introduction

The synthesis of acrylonitrile analogs has been pursued in recent years due to their unique chemical properties. They are a polyfunctional class of molecules containing single, double and triple bonds, in particular, vinyl and cyano groups are considered two of the most important building blocks in organic synthesis [1]. Synthetic approaches to this class of molecules involve Wittig reactions [2,3], McMurry coupling reactions [4], Heck reactions [5], and more recently, condensation reactions of the Knoevenagel type, using acid or base-catalyzed condensation of active methylene moieties with carbonyl compounds [6–9]. In addition, the use of transition metal catalysts such as Pd, Cu, Ni and Co, has also been described [10–12]. Acrylonitrile derivatives bearing heterocyclic cores such as thiazoles [13], pyrazoles [14], benzimidazoles [15], triazolopyridines [16], and benzotriazoles [17], are considered valuable compounds and their biological activities, including anticancer [18], antituberculosis [19], antibacterial [20], and antiproliferative [21], have been demonstrated in the literature.

The benzotriazole structural motif is also an important pharmacophore in many biologically active molecules, and thus the synthesis of compounds bearing this group has received significant interest [22]. Many bioactive heterocyclic compounds that contain a benzotriazole fragment have exhibited outstanding properties in medicinal chemistry including anticancer, antifungal, antibacterial, antiviral, antiparasitic, and antioxidative activities [23]. Furthermore, the benzotriazole ring system also undergoes a unique tautomerism phenomenon between the 1*H*- and 2*H*- forms, where the 1*H*-benzotriazole is the most stable in the solid state and in solution [24,25].

The structural characteristics that allow benzotriazoles to form hydrogen bonds and/or other type of molecular interactions, such as π-π stacking and van der Waals forces, makes them capable of binding with enzymes and receptors in biological systems [22]. For the benzotriazolyl

* Corresponding author.
** Corresponding author.
E-mail addresses: eugenio.hernandezfr@uanl.edu.mx (E. Hernández-Fernández), dmichaelis@chem.byu.edu (D.J. Michaelis).

https://doi.org/10.1016/j.dyepig.2021.109251
Received 8 June 2020; Received in revised form 4 February 2021; Accepted 17 February 2021
Available online 23 February 2021

acrylonitriles presented in this report, the combined presence of an electron-rich donor (*p*-substituted benzaldehydes and benzotriazole units) and an electron-deficient acceptor (cyano group) enables the selective tuning of the photophysical and electronic properties of our chromophores, resulting in a donor-acceptor (D-A) conjugated molecular system [26,27]. In fact, D-A systems with several donor and acceptor units have been reported for applications in chemistry, physics, materials science, and biology, including their use in solar cells [28,29], organic light-emitting diodes (OLEDs) [30,31], metal ions sensors [32–34], polymer staining applications [35], and as markers in security documents [36,37]. Among them, the ability to dye cellular structures for imaging purposes *via* fluorescence is of interest in the medical field due to the valuable readout it can contribute to cell-based assays. Recent advances of this technology include immunoassays that analyze signaling pathways [38], screening for toxic chemicals [39], specific organelle targeting and tracking [40], monitoring of cell states [41], sensor and chemodosimeter studies of specific endogenous reactive oxygen species (ROS) [42–44] and detecting metal ions in cancerous cells [45].

In this sense, the synthesis of D-A molecules based on acrylonitrile derivatives has received great attention in recent years due to their chemical and biological properties; however, the synthesis of most of these types of compounds involve various reaction steps, long reaction times, and poor overall chemical yields. Therefore, the design and synthesis of low-molecular weight compounds that present negligible cytotoxicity and photophysical properties that enable them to be used as cellular markers, continues to be an area of great interest today.

Taking the above precedence into account, our research groups designed and synthesized a series of eight benzotriazolyl acrylonitrile derivatives **6a-d** and **7a-d** *via* Knoevenagel condensation (Scheme 1). The compounds were fully characterized by NMR experiments (^{1}H and ^{13}C) and by high resolution mass spectrometry (HRMS). The optical properties of all the compounds were evaluated and the crystallographic data was obtained for one compound (**7b**) to confirm the double bond geometry of the product. Cytotoxicity was also determined, and confocal microscopy characterization provide evidence for the utility of compounds like **7b** for bioimaging applications.

2. Results and discussion

2.1. Synthesis of benzotriazolyl acrylonitriles *6a-d* and *7a-d*

The preparation of our desired benzotriazole derivatives **6a-d** and **7a-d** was conducted after obtaining their respective precursors **3** and **4** *via* bimolecular nucleophilic substitution (S_N2) between benzotriazole **1** and bromoacetonitrile **2.** Sonication in an ultrasonic bath led to much faster reactions due to the presence of insoluble base (K_2CO_3) in the reaction, and product could be obtained in high yield in as little as 2 h (Scheme 2). The crude reaction mixture was purified by column chromatography to give benzotriazole isomers **3** and **4** (75% vs 25%), which result from the tautomeric effect of the benzotriazole unit. It's important to remark that 1*H*-isomer **3** is formed preferentially due to its higher stability in the tautomeric form.

With the compounds **3** and **4** in hand, the next step was to use both benzotriazolyl acetonitrile isomers for the preparation of the acrylonitrile derivatives **6a-d** and **7a-d** *via* Knoevenagel condensation. Several *p*-substituted benzaldehydes with donor groups were screened in the reaction, including 4-(4-morpholinyl)benzaldehyde, 4-(dimethylamino)benzaldehyde, 4-(diethylamino)benzaldehyde and 4-(diphenylamino)benzaldehyde **5a-d.** Good yields of the desired products (42–78%) were obtained after a short reflux (2 h) in ethanol in presence of piperidine as base (Scheme 3). Compounds **6a-b** and **7a-d** were obtained as yellow and orange solids and compounds **6c** and **6d** as yellow and orange oils, respectively. Most of the products were obtained in pure form and in good yields *via* filtration and washing of the resulting solids from the reaction. The resulting benzotriazolyl acrylonitrile analogs were soluble in common organic solvents such as acetonitrile, methanol, ethanol, chloroform, ethyl acetate, dichloromethane, and dimethyl sulfoxide but insoluble in hexane.

The chemical structure of each compound was fully characterized by ^{1}H NMR and ^{13}C NMR and HRMS. ^{1}H NMR data showed that vinylic protons for compounds **6a-d** appeared in a chemical shift within the range from δ 7.62–7.78 ppm, while their corresponding isomers **7a-d** show those resonance signal with a slight displacement to higher frequency regions (δ 8.35–8.39 ppm). It is noteworthy that compounds **6d** and **7d**, which incorporate the diphenylamino group in their structure, exert a greater deshielding effect on vinylic proton as can be seen in Table 1.

2.2. Single-crystal X-ray diffraction analyses

The spectroscopic analysis of our benzotriazole products was not sufficient at this stage to determine with confidence the geometry of the double bond. Thus, in order to gain a better understanding of the structure of our products, we grew X-ray-quality single crystals of compound **7b**, through slow evaporation of ethyl acetate/hexane solution at room temperature. The crystal structure of **7b** confirmed the (*E*)-geometry of the double bond and the highly planar nature of this class of conjugated system (Fig. 1).

Compound **7b** belongs to the triclinic space group P-1 and crystallizes with two chemically similar but crystallographically different molecules in the unit cell as shown in Fig. 2. The bond angle of N2–C10–C11 (178.9°) with torsion angle of N3–C10–C9–C6 (−178.6°) demonstrate that nitrile is a perfect linear group, which formed a delocalization unit along the phenyl ring and double bond. In addition, the dimethylamine group is also coplanar with the attached phenyl ring, that is parallel to the benzotriazole unit.

In the crystal, molecules are stacked through C2–H2B···N5 weak interactions (d = 2.741 Å) within the 1D framework as shown in Fig. 3.

Detailed crystallographic parameters are included in Table 2.

2.3. Optical properties

The optical properties of 1*H*-benzotriazolyl acrylonitrile derivatives **6a-d** and their corresponding 2*H*-tautomers **7a-d** were next studied (Table 3). Fig. 4a shows the electronic absorption spectra of 1*H*-benzotriazolyl acrylonitrile derivatives **6a-d**, and Fig. 4b shows those corresponding to 2*H*-tautomers **7a-d**. In general, all the benzotriazolyl acrylonitrile derivatives exhibit a main absorption band with maximum wavelength ranging between 383 and 434 nm, which can be attributed

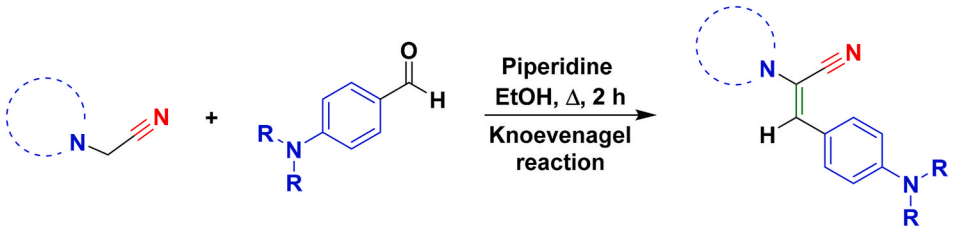

Scheme 1. Designed and synthesized compounds in this work.

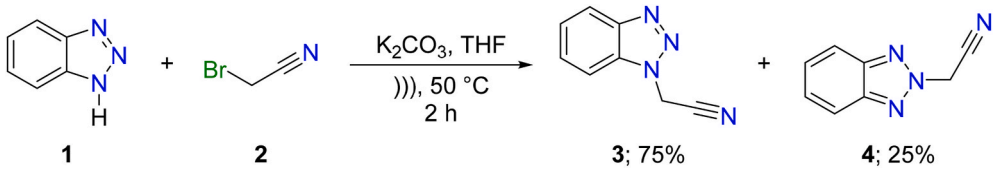

Scheme 2. Synthesis of benzotriazolyl acetonitriles **3** and **4**.

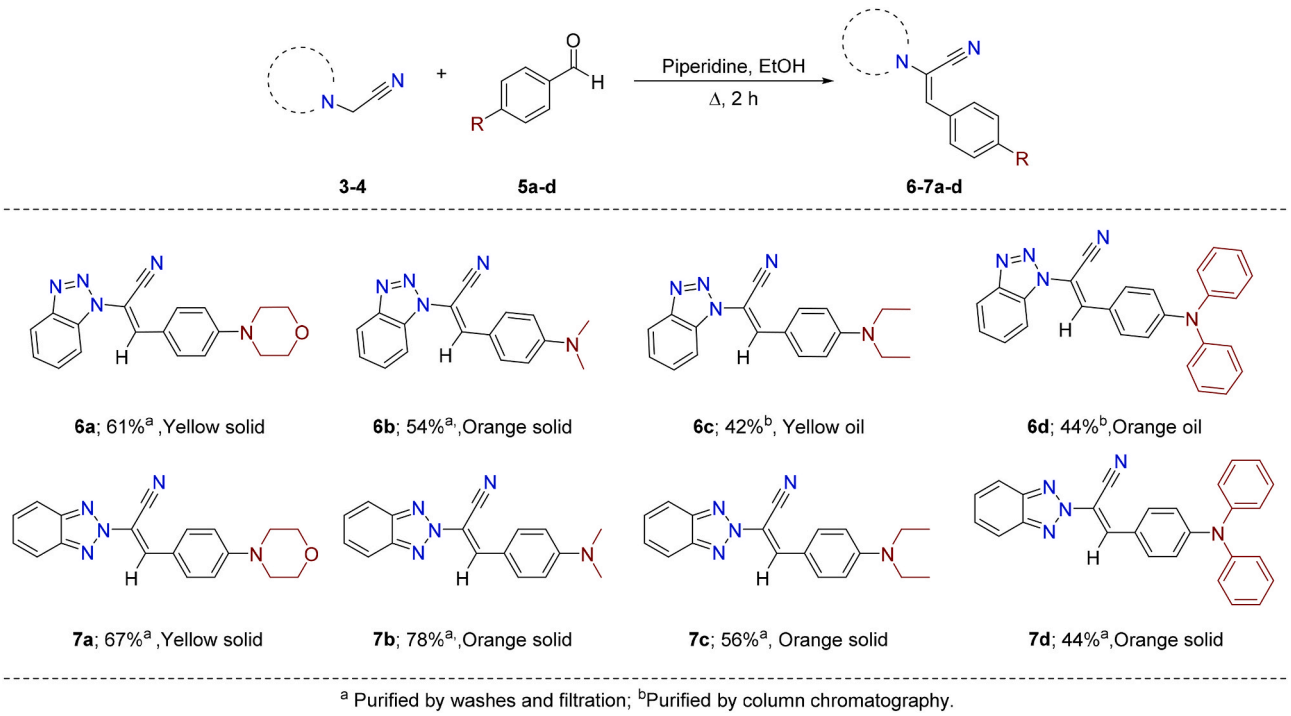

Scheme 3. Synthesis of benzotriazolyl acrylonitrile analogs **6a-d** and **7a-d**.

Table 1
^{1}H NMR spectroscopic data for vinylic protons in compounds **6a-d** and **7a-d**.

Compound	vinylic proton (δ, ppm)	Compound	vinylic proton (δ, ppm)
6a	7.72	**7a**	8.37
6b	7.66	**7b**	8.36
6c	7.62	**7c**	8.35
6d	7.78	**7d**	8.39

to the π→π* (HOMO-LUMO) electronic transition. The position of the maximum depends on the electronic delocalization through molecules in both series. This delocalization is chemically modulated by varying the electron donating groups in the *para* position of the terminal phenyl ring (morpholinyl for **6a** and **7a**, dimethyl (diethyl) for **6b** and **7b** (**6c** and **7c**), or diphenyl for **6d** and **7d**) and by the nitrile electron withdrawing group. In accordance with strong electron donating ability of dimethyl (diethyl)amine compared to morpholine, the main absorption bands of **6b** and **7b** (**6c** and **7c**) exhibit a bathochromic shift compared to **6a** and **7a**. Likewise, the lowest energy bands of the compounds with diethylamine group (**6c** and **7c**) appear at slightly higher energies in relation to those reported for **6d** and **7d**, substituted with diphenylamine groups. We found that **6d** and **7d** exhibit a bathochromic behavior with respect to those of **6c** and **7c** due to their higher π-delocalization, as has been previously reported for trisheterocyclic systems with electron donating amino groups [46]. The maximum absorption is also affected by changing the position of the double bond on the benzotriazole from the 1*H* or the 2*H*-tautomer. We found that the different electron donating groups clearly affect the conjugated styryl segment, as has been previously reported for fluorescent salicylidenebenzoylhydrazones [47]. For benzotriazolyl acrylonitrile **6c** a shoulder at 344 nm is also evident and has been attributed to an n→π* transition of the nitrile electron withdrawing group for similar molecules with donor-acceptor design [48]. On varying the solvent polarity from aprotic to protic from chloroform to acetonitrile and methanol, the shift of the longest wavelength absorption band was so smaller than 7 nm (Table 3, Table ESI-5, Fig. ESI-18, and Fig. ESI-19). This poor solvatochromic response indicates the solvent do not affect the intramolecular interaction between donor and acceptor groups in the ground state. Accordingly, the optical band gap Eg_{opt}, which is in the semiconducting range for all these molecules, decreases from 3.23 to 2.86 eV as the electron donating character increases in each series.

The fluorescence spectra of 1*H*-benzotriazolyl acrylonitrile derivatives **6a-d** and their corresponding 2*H*-tautomers **7a-d** are shown in Fig. 5. Benzotriazolyl acrylonitriles **6a-c** and their corresponding 2*H*-tautomers **7a-c** show broad blue and green emission bands in the 485–524 nm range, while derivatives **6d** and **7d** exhibit a broad yellow peak, in agreement with the hypsochromic shift observed in the corresponding absorption spectra. Moreover, the excitation and absorption spectra are identical, which is consistent with the existence of just one emitting state (benzotriazolyl acrylonitriles **6a-d** as examples in Fig. ESI-20).

An interesting fact is that the emission can be tuned from the blue (**6a**, **6b** and **7a**) to the green (**6c**,**d**, and **7b**,**c**) and yellow (**7d**) regions by changing the electron-donating substituents in the *para* position on the styryl ring. Stokes' shift values are in the range of molecules that dramatically change their geometry after excitation with non-radiative

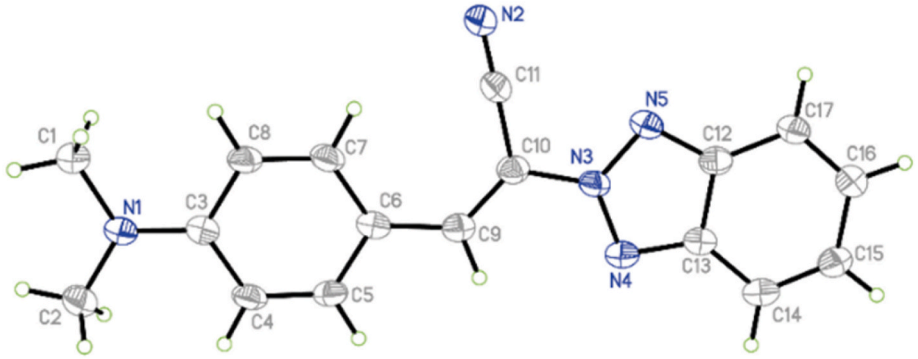

7b

Fig. 1. Molecular structure of benzotriazolyl acrylonitrile **7b** (CCDC 1864140) as determined by single-crystal X-ray diffraction analysis.

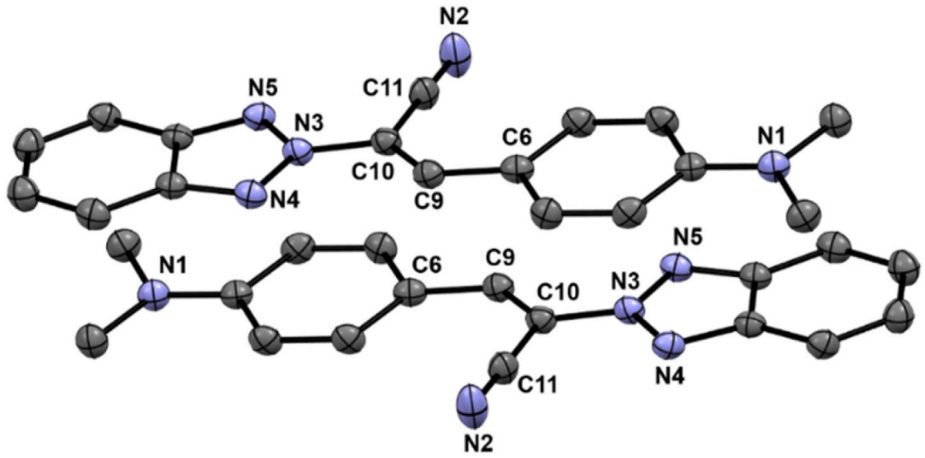

Fig. 2. Anisotropic displacement parameters depicted at the 50% probability level. Hydrogen atoms were omitted for clarity. Selected bond distances (Å) and angles (°): N3–C10 = 1.412(2); C10–C11 = 1.436(2); C6–C9 = 1.440(3); C9–C10 = 1.352(2); N2–C11 = 1.352(2); N3–C10–C9 = 122.5(1); C6–C9–C10 = 130.2(1); N3–C10–C11 = 112.6(1).

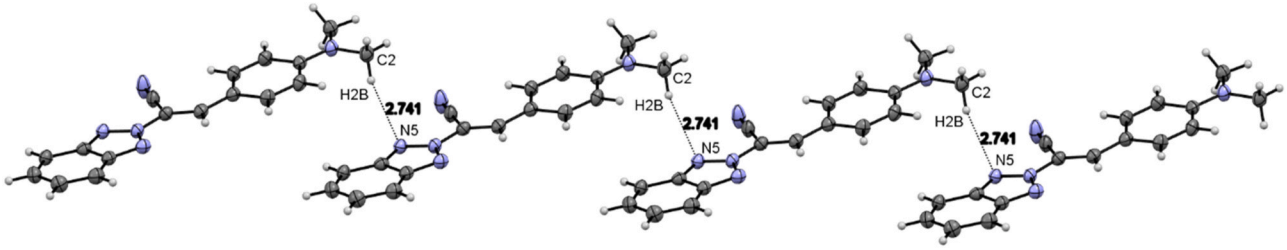

Fig. 3. The 1D framework shown C2–H2B···N5 interaction within the crystal structure.

losses associated to fluorescence quenching [49]. On the other hand, the low quantum yield measured under our experimental conditions [47,50] could be related due to charge transfer from the electron-donating –N $(CH_2CH_2)_2O$, -Me_2N (-Et_2N) or -Ph_2N to electron-acceptor (C≡N) groups, and by the donor character of benzotriazole group in the compounds. Furthermore, the X-ray diffraction analyses for **7b**, showed that the relative face to face stacking distance of pairs of molecules was 7.438 Å (Fig. ESI-17), which could also explain the low quantum yield, as previously reported by Xue et al. for cyano-stilbene derivatives with alkyl group, where the authors found that compounds without π-π stacking and coplanar arrangement exhibit high quantum yields [51]. Consequently, the elimination of either the benzotriazole (electron-donating) or the nitrile (electron-withdrawing) groups, present in the structure of this type of compounds, will allow us to get a better understanding of its photophysical properties (fluorescence quantum yields), which are in progress and they will be reported in future studies.

Regarding fluorescence quantum yield, compounds showed values in the 0.05–0.58% range, where a slightly higher φ value in solution was found for most of the 2*H*-benzotriazolyl acrylonitrile derivatives (**7a-c**) in comparison to their 1*H*-tautomers (**6a-c**), except for **7d**, which

Table 2
Selected crystal data for compound **7b**.

Compound	**7b**
Chemical formula	$C_{17}H_{15}N_5$
M	289.34 g/mol
Crystal system	Triclinic
Space group	P-1
A	7.4380(6) Å
B	10.2915(6) Å
C	10.7640(7) Å
α	65.377(4)°
β	82.735(5)°
γ	71.907(4)°
V	712.00(9) Å^3
R_1	0.0414
wR_2	0.1151
Z	2
CCDC ID	1864140

Table 3
Optical properties of benzotriazolyl acrylonitrile derivatives **6a-d** and **7a-d** in CH_3CN.

Molecule	λ_{abs} (nm)	ε (10^4 M^{-1} cm^{-1})	Eg_{opt} (eV)	λ_{emi} (nm)	$\Delta\nu$ (cm^{-1})	φ (%)	SS (nm)
6a	383	6.07	3.23	485	5491	0.08	102
6b	394	6.49	3.14	490	4973	0.05	96
6c	401	6.67	3.09	492	4412	0.09	91
6d	406	7.39	3.05	555	6612	0.58	149
7a	395	5.72	3.14	521	6122	0.15	126
7b	400	4.90	3.10	523	5880	0.12	123
7c	407	7.40	3.04	524	5486	0.11	117
7d	434	3.18	2.86	577	5710	0.55	143

showed a slightly lower value compared to **6d**. However, according to the desirable spectroscopic and photophysical criteria for bioimaging applications, including absorption in the visible region (>400 nm), high absorption coefficient (>30 000 M^{-1} cm^{-1}), and large Stokes shift (typically over 100 nm), our compounds successfully meet these requirements. The importance of this latter relies in the fact that a large value helps to minimize cross-talk between the excitation source and the fluorescent emission with high signal-to noise ratio. It also is useful to avoid reabsorption of emitted photons leading to undesired background interferences that might give false positive results and is critical to the extremely high sensitivity of fluorescence imaging measurements [52–55].

2.4. In vitro cytotoxicity and cell imaging

To determine the suitability of these compounds for use in cell-based analysis, we decided to perform a screening only for the compound **7b** due to its good chemical yield (78%), high ε (49 000 M^{-1} cm^{-1}), λ_{abs} (400 nm), and large Stokes' shift value (123 nm). Cytotoxicity assays were performed by co-incubating various concentrations of this compound with HEK 293T cells, a common mammalian cell line, and determining cell viability after 24 h. The results of this assay showed limited toxicity of compound **7b** for these cells up to 50 μM, the maximum tested concentration. Even at this concentration, the cells maintained 72 ± 16% viability, indicating that the LC50 is similar to or exceeds this value (Fig. 6). Many other "cell-safe" fluorophore constructs, such as Rhodamine 6G and PEI-$DOCA_{20}$-Cy5.5, exhibit similar or higher toxicities [56,57]. Therefore, compound **7b** presents little risk of toxicity in mammalian cell-based assays.

Following cytotoxicity screening, we assessed how compound **7b** was internalized by cells and whether it localized to specific cellular compartments, as occurred with similar compounds [58]. Therefore, we co-incubated compound **7b** in cell culture with dextran–Cascade Blue (DCB), a 10 kD polysaccharide–fluorophore conjugate, and characterized localization of both **7b** and DCB by confocal microscopy (Fig. 7). DCB localizes to endosomes and lysosomes and is an effective marker of these compartments within the cell [59,60]. We observed that compound **7b** co-localized broadly with DCB in HEK 293T cells, indicating that **7b** localizes to endosomes and/or lysosomes in a similar fashion to DCB. A modified experiment (pulse-chase condition), in which DCB was removed from cell media 4 h before imaging, sequesters DCB in lysosomes alone [61]. When this experiment was performed, DCB once again co-localized with compound **7b**, indicating that it is trafficked to lysosomes, like DCB. These data indicate that **7b** is a membrane-impermeable, fluid-phase marker like DCB.

The unique structure and excitation/emission profile of compound **7b**, as compared to many other fluorophores, may provide special utility as a cell-based fluorescent marker. Many fluorophores can be excited at 405 nm, but only a few emit near 550 nm as compound **7b** does [62]. This large Stokes' shift, together with its low cytotoxicity, may prove useful for both fluorescence microscopy and flow cytometry for labeling endosomes and lysosomes in cell-based assays. Due to its chemical structure, it is anticipated that derivatization of compound **7b** could be performed to increase its utility in biological assays without introducing substantial changes in the spectral character of the molecule.

3. Conclusions

In this work, we present a straightforward and fast synthetic method to obtain benzotriazolyl acrylonitrile derivatives with yields from 42%

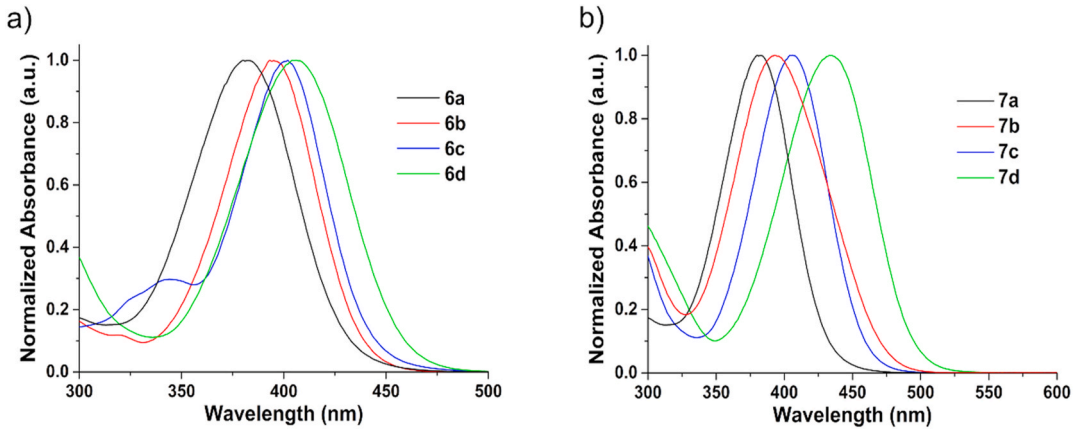

Fig. 4. Absorption spectra of a) **6a-d** and b) **7a-d** benzotriazolyl acrylonitrile derivatives in CH_3CN at 25 °C at concentrations from 1.90 to 2.80 × 10^{-4} M.

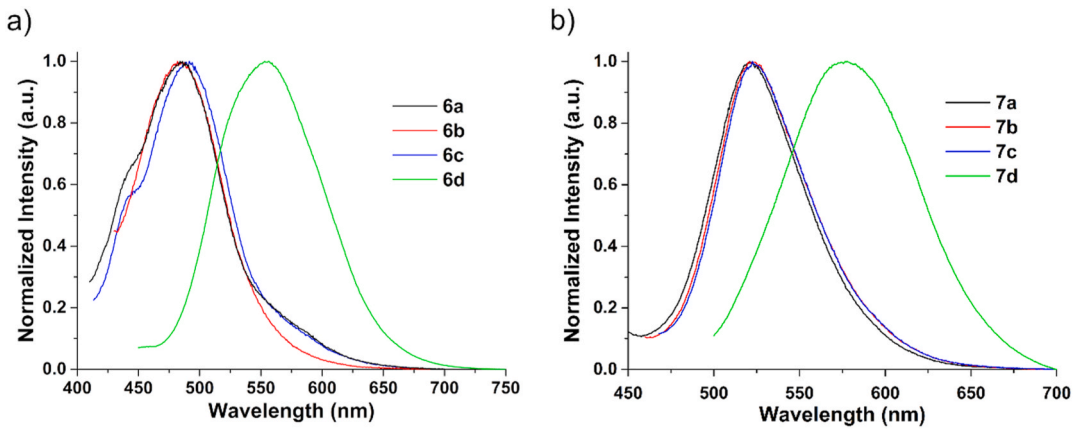

Fig. 5. Emission spectra of a) **6a-d** and b) **7a-d** benzotriazolyl acrylonitrile derivatives in CH_3CN at 25 °C at concentrations from 10^{-4} to 10^{-6} M.

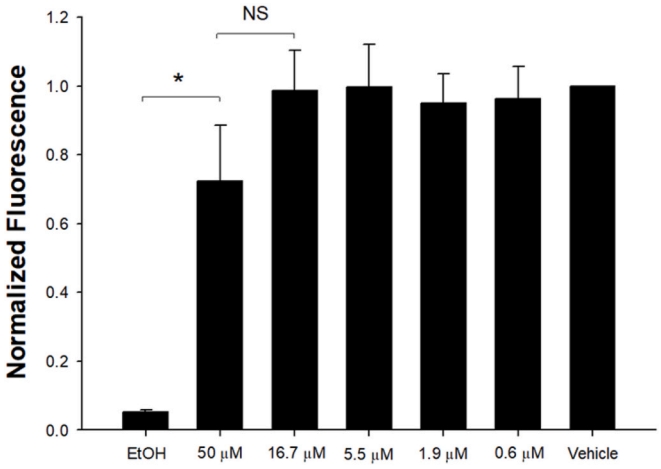

Fig. 6. Cytotoxicity of compound **7b** was assayed at concentrations from 0.6 to 50 μM. A decrease in cell viability compared to vehicle only control was only noted in the 50 μM treatment condition, which was not statistically significant ($p = 0.24$). The positive control (EtOH killed cells) was significantly lower than all other conditions. *, $p < 0.05$; NS, not significant.

to 78%. Our synthetic protocol benefits from the fact that most of our products are easily purified by washing and filtration using ethanol. The (*E*)-geometry of the double-bond was confirmed for compound **7b** by single-crystal X-ray diffraction. The optical properties showed that all the compounds presented a low quantum yield of fluorescence from 0.05% to 0.58%; however, compounds **6a**, **6d**, and **7a-d** presented a large Stokes' shift (greater than 100 nm) in fluorescence studies. Based on this characteristic, compound **7b** was selected to further determine its toxicity to a common mammalian cell line (HEK 293T cells) and its localization within these cells upon uptake. The results showed that **7b** has low toxicity and is internalized by cells and localized into endosomes and/or lysosomes. Up to this point, these studies demonstrated that compound **7b** could be used as a cell-based fluorescent marker. Additionally, these types of derivatives could be further studied to confirm their suitability to act as promising tools for fluorescent applications in biological, medical, and other chemistry related fields.

4. Experimental section

4.1. Synthesis and characterization

All starting chemicals were obtained commercially as analytical reagent and used directly without any purification. Melting points were determined on an Electrothermal Mel-Temp apparatus and are uncorrected. Thin-layer chromatography was performed on pre-coated sheets of silica gel 60 F254 (E. Merck). For column chromatography 230–400 mesh silica gel 60 (E. Merck) was used as stationary phase. Proton nuclear magnetic resonance (^{1}H NMR) data were acquired on an Inova 300 MHz or a Bruker 400 MHz. Chemical shifts are reported in delta (δ) units. Signals are reported as follows: s (singlet), d (doublet), t (triplet), q (quartet), m (multiplet). Coupling constants are reported in hertz (Hz). Carbon-13 nuclear magnetic resonance (^{13}C NMR) data were acquired on an Inova at 75 MHz or Bruker 100 MHz spectrometer. Chemical shifts are reported in ppm. Mass spectral data were obtained using ESI techniques (Agilent, 6210 TOF).

4.1.1. Procedure for the synthesis of benzotriazolyl acetonitriles *3* and *4*

Benzotriazole **1** (1 equiv), K_2CO_3 (2.2 equiv) and dry THF (30 mL) were combined in a 250 mL flask. Then, bromoacetonitrile **2** (1.2 equiv) was added dropwise and the reaction was left under an ultrasound bath for 2 h. Reaction course was monitored by TLC analysis. After completion of the reaction, the solvent was removed, and the reaction mixture was washed with water and extracted with ethyl acetate (3 × 30 mL). The organic layer was dried over anhydrous Na_2SO_4 and concentrated under reduced pressure. Isolation of both isomer products was accomplished by column chromatography using a hexane/EtOAc (2:1) system.

4.1.1.1. 2-(1H-benzo[d][1,2,3]triazol-1-yl)acetonitrile ***3***. (75%) Beige solid, mp 86–87 °C; ^{1}H NMR (400 MHz, CD_3OD): δ 5.96 (s, 2H, CH_2CN), 7.44–7.48 (m, 1H, H_{arom}), 7.59–7.63 (m, 1H, H_{arom}), 7.82 (d, $J = 8.4$ Hz, 1H, H_{arom}), 8.01 (d, $J = 8.4$ Hz, 1H, H_{arom}); ^{13}C NMR (100 MHz, CD_3OD): δ 36.4, 110.7, 114.9, 120.5, 126.1, 129.8, 133.9, 146.8. HRMS (ESI^+) calcd for $C_8H_7N_4$ $[M+H]^+$ 159.06707, found 159.06712. Lit [63].

4.1.1.2. 2-(2H-benzo[d][1,2,3]triazol-2-yl)acetonitrile ***4***. (25%) Beige solid, mp 78–80 °C; ^{1}H NMR (500 MHz, $CDCl_3$): δ 5.68 (s, 2H, CH_2), 7.44–7.46 (m, 2H, H_{arom}), 7.87–7.89 (m, 2H, H_{arom}); ^{13}C NMR (125 MHz, $CDCl_3$): 43.6, 112.3, 118.2, 127.7, 145.1. HRMS (ESI^+) calcd for $C_8H_7N_4$ $[M+H]^+$ 159.06707, found 159.06716. Lit [19,21].

4.1.2. General procedure for the synthesis of benzotriazolyl acrylonitriles *6a-d, 7a-d*

Precursor benzotriazolyl acetonitrile **3** or **4** (1 equiv) and piperidine (1.0 equiv) were dissolved in ethanol (30 mL) and stirred vigorously for 10 min at room temperature. Then, corresponding aldehyde **5a-d** (1.0 equiv) was added to the solution and reacted under reflux for 2 h. The course of the reaction was monitored by TLC (7:3 hexane/EtOAc). After solvent evaporation under vacuum, the crude product was filtered and washed with ethanol. For derivatives **6c** and **6d**, the crude product was purified on column chromatography using a hexane/EtOAc (9:1) eluent system. Yields, melting points (mp) and spectroscopic data are reported

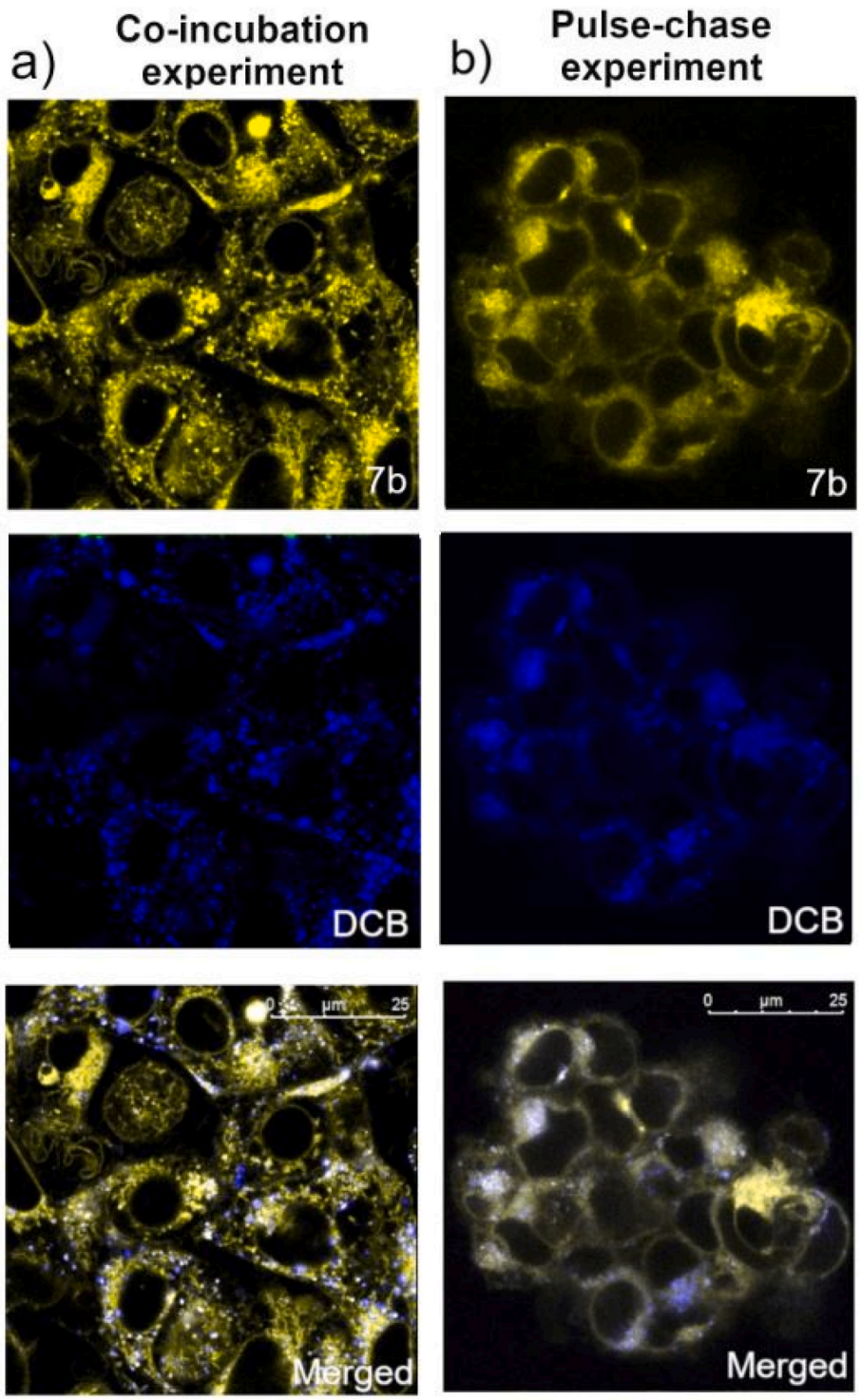

Fig. 7. a) Compound **7b** (10 μM) was co-incubated in cell media with DCB (50 μM) and showed colocalization with DCB, suggesting that it also is present in endosomes and lysosomes. b) In a modified assay (pulse-chase condition), DCB was removed from the cell medium 4 h before imaging, leaving DCB primarily in lysosomes. Close analysis of the images reveals accumulation of both compound **7b** and DCB in discrete puncta within the cell.

as follows:

4.1.2.1. (E)-2-(1H-benzo[d][1,2,3]triazol-1-yl)-3-(4-morpholinophenyl) acrylonitrile ***6a****.* (60%) Yellow solid, mp 207–208 °C, ^{1}H NMR (300 MHz, $CDCl_3$): δ 3.35 (t, $J = 4.4$ Hz, 4H, $(CH_2)_2N$), 3.90 (t, $J = 4.6$ Hz, 4H, $(CH_2)_2O$), 6.94 (d, $J = 8.7$ Hz, 2H, H_{arom}), 7.46 (m, 2H, H_{arom}), 7.72 (s, 1H, $H_{vinylic}$), 7.85–7.89 (m, 3H, H_{arom}), 8.12 (d, $J = 8.3$ Hz, 1H, H_{arom}); ^{13}C NMR (75 MHz, $CDCl_3$): δ 47.4, 66.6, 101.8, 110.3, 114.2, 114.9, 118.2, 120.6, 125.0, 127.8, 128.9, 131.9, 141.8, 146.3, 153.5. HRMS (ESI^+) calcd for $C_{19}H_{18}N_5O$ $[M+H]^+$ 332.15114, found 332.14883.

4.1.2.2. (E)-2-(1H-benzo[d][1,2,3]triazol-1-yl)-3-(4-(dimethylamino) phenyl)acrylonitrile ***6b****.* (45%) Orange solid, mp 186–188 °C, ^{1}H NMR (300 MHz, $CDCl_3$): δ 3.10 (s, 6H, $(CH_3)_2$), 6.74 (d, $J = 9.0$ Hz, 2H, H_{arom}), 7.42–7.47 (m, 1H, H_{arom}), 7.56–7.61 (m, 1H, H_{arom}), 7.66 (s, 1H, $H_{vinylic}$), 7.84 (d, $J = 8.3$ Hz, 1H, H_{arom}), 7.86 (d, $J = 9.0$ Hz, 2H, H_{arom}),

8.12 (d, $J = 8.4$ Hz, 1H, H_{arom}); ^{13}C NMR (75 MHz, $CDCl_3$): δ 40.1, 99.5, 110.4, 111.8, 115.6, 117.7, 120.5, 124.8, 128.7, 132.1, 132.3, 143.0, 146.2, 152.8. HRMS (ESI^+) calcd for $C_{17}H_{16}N_5$ $[M+H]^+$ 290.14057, found 290.14083.

4.1.2.3. (E)-2-(1H-benzo[d][1,2,3]triazol-1-yl)-3-(4-(diethylamino) phenyl)acrylonitrile ***6c.*** (42%) Yellow oil, ^1H NMR (300 MHz, $CDCl_3$): δ 1.23 (t, $J = 7.1$ Hz, 6H, $(CH_2CH_3)_2$), 3.45 (q, $J = 7.1$ Hz, 4H, $(CH_2CH_3)_2$), 6.72 (d, $J = 9.0$ Hz, 2H, H_{arom}), 7.42–7.47 (m, 1H, H_{arom}), 7.55–7.61 (m, 1H, H_{arom}), 7.62 (s, 1H, $H_{vinylic}$), 7.83 (d, $J = 8.4$ Hz, 1H, H_{arom}), 7.84 (d, $J = 9.0$ Hz, 2H, H_{arom}), 8.11 (d, $J = 8.4$ Hz, 1H, H_{arom}); ^{13}C NMR (175 MHz, $CDCl_3$): δ 12.7, 44.8, 98.9, 110.4, 111.4, 115.8, 117.1, 120.5, 124.8, 128.7, 132.4, 132.5, 143.1, 146.2, 150.7. HRMS (ESI^+) calcd for $C_{19}H_{20}N_5$ $[M+H]^+$ 318.17187, found 318.17058.

4.1.2.4. (E)-2-(1H-benzo[d][1,2,3]triazol-1-yl)-3-(4-(diphenylamino) phenyl)acrylonitrile ***6d.*** (44%) Orange oil, ^1H NMR (300 MHz, $CDCl_3$): δ 7.10 (d, $J = 8.8$ Hz, 2H, H_{arom}), 7.21–7.24 (m, 6H, H_{arom}), 7.36–7.41 (m, 4H, H_{arom}), 7.47–7.53 (m, 1H, H_{arom}), 7.62–7.67 (m, 1H, H_{arom}), 7.78 (s, 1H, $H_{vynilic}$), 7.82 (d, $J = 8.8$ Hz, 2H, H_{arom}), 7.91 (d, $J = 8.4$ Hz, 1H, H_{arom}), 8.16 (d, $J = 8.4$ Hz, 1H, H_{arom}); ^{13}C NMR (75 MHz, $CDCl_3$): δ 102.4, 110.4, 114.8, 120.2, 120.6, 122.4, 125.0, 125.2, 126.3, 126.3, 128.9, 129.8, 129.9, 131.4, 141.4, 146.2, 151.5; HRMS (ESI^+) calcd for $C_{27}H_{20}N_5$ $[M+H]^+$ 414.17187, found 414.17294.

4.1.2.5. (E)-2-(2H-benzo[d][1,2,3]triazol-2-yl)-3-(4-morpholinophenyl) acrylonitrile ***7a.*** (67%) Yellow solid, mp 241–243 °C, ^1H NMR (300 MHz, $CDCl_3$): δ 3.33 (t, $J = 4.6$ Hz, 4H, $(CH_2)_2N$), 3.86 (t, $J = 4.5$ Hz, 4H, $(CH_2)_2O$), 6.92 (d, $J = 9.0$ Hz, 2H, H_{arom}), 7.41–7.44 (m, 2H, H_{arom}), 7.88–7.94 (m, 4H, H_{arom}), 8.37 (s, 1H, $H_{vynilic}$); ^{13}C NMR (75 MHz, $CDCl_3$): δ 47.3, 66.6, 108.2, 114.2, 114.3, 118.2, 120.4, 127.8, 132.2, 137.4, 144.9, 153.4. HRMS (ESI^+) calcd for $C_{19}H_{18}N_5O$ $[M+H]^+$ 332.15114, found 332.14907.

4.1.2.6. (E)-2-(2H-benzo[d][1,2,3]triazol-2-yl)-3-(4-(dimethylamino) phenyl)acrylonitrile ***7b.*** (78%) Orange solid, mp 254–256 °C, ^1H NMR (300 MHz, $CDCl_3$): δ 3.09 (s, 6H, $(CH_3)_2$), 6.73 (d, $J = 9.1$ Hz, 2H, H_{arom}), 7.40–7.43 (m, 2H, H_{arom}), 7.88–7.93 (m, 2H, H_{arom}), 8.36 (s, 1H, $H_{vynilic}$); ^{13}C NMR (75 MHz, $CDCl_3$): δ 40.2, 106.4, 111.9, 114.9, 117.6, 118.1, 127.5, 132.5, 138.1, 144.8, 152.7. HRMS (ESI^+) calcd for $C_{17}H_{16}N_5$ $[M+H]^+$ 290.14057, found 290.13784.

4.1.2.7. (E)-2-(2H-benzo[d][1,2,3]triazol-2-yl)-3-(4-(diethylamino) phenyl)acrylonitrile ***7c.*** (34%) Orange solid, mp 190–191 °C, ^1H NMR (300 MHz, $CDCl_3$): δ 1.23 (t, $J = 7.1$ Hz, 6H, $(CH_2CH_3)_2$), 3.45 (t, $J = 7.1$ Hz, 4H, $(CH_2CH_3)_2$), 6.71 (d, $J = 9.1$ Hz, 2H, H_{arom}), 7.40–7.43 (m, 2H, H_{arom}), 7.88–7.91 (m, 4H, H_{arom}), 8.35 (s, 1H, $H_{vynilic}$); ^{13}C NMR (75 MHz, $CDCl_3$): δ 12.7, 44.8, 105.9, 111.5, 115.1, 116.9, 118.0, 127.4, 132.9, 138.1, 144.8, 150.6. HRMS (ESI^+) calcd for $C_{19}H_{20}N_5$ $[M+H]^+$ 318.17187, found 318.16926.

4.1.2.8. (E)-2-(2H-benzo[d][1,2,3]triazol-2-yl)-3-(4-(diphenylamino) phenyl)acrylonitrile ***7d.*** (43%) Orange solid, mp 180–181 °C, ^1H NMR (300 MHz, $CDCl_3$): δ 7.05 (d, $J = 8.8$ Hz, 2H, H_{arom}), 7.15–7.21 (m, 6H, H_{arom}), 7.33–7.45 (m, 6H, H_{arom}), 7.82–7.92 (m, 6H, H_{arom}), 8.39 (s, 1H, $H_{vynilic}$); ^{13}C NMR (75 MHz, $CDCl_3$): δ 108.8, 114.2, 118.2, 120.2, 122.2, 125.2, 126.3, 127.9, 129.9, 131.8, 137.1, 145.0, 146.2, 151.4. HRMS (ESI^+) calcd for $C_{27}H_{20}N_5$ $[M+H]^+$ 414.1787, found 414.16978.

4.2. Single-crystal X-ray diffraction analyses

Compound **7b** was crystallized using slow evaporation in EtOAc/hexanes to produce yellow single crystals for X-ray diffraction experiments. High-resolution (0.84 °A) data were collected at 100 K using Cu-Kα radiation produced by a Bruker-Nonius FR591 rotating anode X-ray source coupled to a MACH3 kappa goniometer and Bruker Apex II CCD detector. The SAINT [64] and SADABS [65] programs, as incorporated in the APEX3 package, were employed to integrate, scale, and correct the obtained data. The structure was solved using dual-space methods in SHELXT [66] and refined against F^2 using SHELXL [67].

4.3. Optical properties

For the photophysical characterization, spectroscopic grade CH_3CN from Aldrich was freshly distilled and the solutions were studied as prepared, in order to avoid any solvolysis or photodegradation effect [68]. UV–Vis absorption and fluorescence spectra were measured on a Varian Cary 100 spectrophotometer and a PerkinElmer LS 50B spectrofluorometer, respectively. The optical band gap (Eg) was determined from the intercept with the X axis of the tangent of the absorption spectrum drawn at absorbance of 0.1. Emission spectra were recorded with a PerkinElmer LS55 spectrofluorometer, by exciting 10 nm below the longer wavelength absorption band. Fluorescence quantum yields (φ) in solution were determined according to the procedure reported in the literature [69], using quinine sulfate in H_2SO_4 0.1 M (φ (%) = 0.54 at 310 nm) as the internal standard. Temperature was regulated at 25.0 ± 0.5 °C with a water circulating bath. Three solutions with absorbance at the excitation wavelength lower than 0.1 were analyzed for each sample and the φ was averaged. φ Measurements were determined by the relative method and the quantum yield of the unknown, φ_x, was calculated according to the following equation:

$$\varphi_x = \varphi_R \cdot \frac{A_R}{A_x} \cdot \frac{E_x}{E_R} \cdot \frac{I_R}{I_x} \cdot \frac{n_x^2}{n_R^2} \quad (1)$$

where φ_R is the quantum yield of the standard, A is the absorbance of the solution, E is the corrected emission intensity, I is the relative intensity of the exciting light and n is the average refractive index of the solution. Subscripts R and X refer to the reference and unknown analyte, respectively.

4.4. In vitro cytotoxicity and cell imaging

For cytotoxicity determination, HEK 293T cells were co-incubated with various concentrations of compound **7b** and cell viability was measured after 24 h *via* resorufin fluorescence. Cells were seeded at 20 000 cells per well in a 96-well, tissue culture-treated optical plate (Nunc). Seeding and incubation were performed in full medium (Dulbecco's Modified Eagle Medium supplemented with 10% fetal bovine serum). After seeding, cells were left for 24 h to adhere to the wells, after which growth media was removed and full medium added, containing various concentrations of compound and up to 1% DMSO. For negative (vehicle) control, cells were incubated with 1% DMSO in full medium alone. Positive (dead) control included a 2 min wash in 85% ethanol/15% H_2O before adding full medium. After a 20 h incubation with compound or vehicle, resazurin in phosphate buffered saline was added at 20 μg mL^{-1} to each well. Cells were then allowed to incubate for an additional 2 h, after which well fluorescence was measured using a BioTek Synergy Hybrid plate reader at 590 nm emission and 560 nm excitation. Normalized values were used to combine datasets; data shown are averages of three independent replicates.

Cell imaging was performed with a Leica DMi8 confocal microscope (Leica Microsystems), exciting at 405 nm for both DCB and compound **7b**, and with emission filters of 420 ± 30 nm and 545 ± 30 nm for DCB and compound **7b**, respectively. HEK 293T cells were treated by co-incubating with 10 μM compound **7b** and 50 μM DCB for 16 h prior to imaging, after which medium was removed. In pulse-chase assays, cells were washed after 12 h with full media and incubated for an additional 4 h in media containing 10 μM compound **7b** only before imaging. Cells were washed once with full medium before imaging. Cells were imaged live in full medium at 37 °C with 100% humidity and 5% CO_2. Cell

images were analyzed and exported using the LAS X Life Science software platform (Leica Microsystems).

Author statement

Eugenio Hernández-Fernández: Conceptualization, Methodology, Validation, Investigation, Resources, Writing – original draft, Writing – review & editing, Funding acquisition; Ana Sofia Ortega-Villarreal: Writing – original draft, Formal analysis; Ma. Concepción García-López: Writing – original draft; Rodrigo Chan-Navarro: Writing – original draft, Formal analysis, Writing – review & editing; Samuel Garrard: Investigation, Writing – original draft; Gabriel A. Valdivia-Berroeta: Formal analysis; Stacey J. Smith: Formal analysis; Kenneth A. Christensen: Methodology, Writing – review & editing; David J. Michaelis: Writing – review & editing, Resources.

Declaration of competing interest

The authors declare that they have no known competing financial interests or personal relationships that could have appeared to influence the work reported in this paper.

Acknowledgements

The authors thank CONACYT of México for the financial support *via* project CB-2015/256359. E.H.F. also thank CONACYT for sabbatical scholarship (472413). S.G. acknowledges support as a Beckman Scholar from the Arnold and Mabel Beckman Foundation.

Appendix A. Supplementary data

Supplementary data to this article can be found online at https://doi.org/10.1016/j.dyepig.2021.109251.

References

[1] Tao F, Sim WS, Xu GQ, Qiao MH. Selective binding of the cyano group in acrylonitrile adsorption on Si(100)-2 × 1. J Am Chem Soc 2001;123:9397–403. https://doi.org/10.1021/ja010574j.
[2] Rocha DHA, Pinto DCGA, Silva AMS. Applications of the Wittig reaction on the synthesis of natural and natural-analogue heterocyclic compounds. Eur J Org Chem 2018;2018:2443–57. https://doi.org/10.1002/ejoc.201800523.
[3] Parthasarathy V, Castet F, Pandey R, Mongin O, Das PK, Blanchard-Desce M. Unprecedented intramolecular cyclization in strongly dipolar extended merocyanine dyes: a route to novel dyes with improved transparency, nonlinear optical properties and thermal stability. Dyes Pigments 2016;130:70–8. https://doi.org/10.1016/j.dyepig.2016.03.008.
[4] Takeda T, Tsubouchi A. The McMurry coupling and related reactions. In: Org. React. vol. 82. Hoboken, NJ, U. S.: Wiley; 2013. p. 1–470. https://doi.org/10.1002/0471264180.or082.01.
[5] Masllorens J, Moreno-Mañas M, Pla-Quintana A, Pleixats R, Roglans A. Stereospecific synthesis of 3,3-disubstituted acrylonitriles by Heck reaction. Synthesis 2002;13:1903–11. https://doi.org/10.1002/chin.200301086.
[6] Parveen M, Malla AM, Alam M, Ahmad M, Rafiq S. Stereoselective synthesis of Z-acrylonitrile derivatives: catalytic and acetylcholinesterase inhibition studies. New J Chem 2014;38:1655–67. https://doi.org/10.1039/c3nj01384g.
[7] Hong Y, Liao JY, Fu J, Kuang D Bin, Meier H, Su CY, et al. Performance of dye-sensitized solar cells based on novel sensitizers bearing asymmetric double D-π-A chains with arylamines as donors. Dyes Pigments 2012;94:481–9. https://doi.org/10.1016/j.dyepig.2012.02.011.
[8] Redon S, Eucat G, Ipuy M, Jeanneau E, Gautier-Luneau I, Ibanez A, et al. Tuning the solid-state emission of small push-pull dipolar dyes to the far-red through variation of the electron-acceptor group. Dyes Pigments 2018;156:116–32. https://doi.org/10.1016/j.dyepig.2018.03.049.
[9] Zhu H, Huang J, Kong L, Tian Y, Yang J. Branched triphenylamine luminophores: aggregation-induced fluorescence emission, and tunable near-infrared solid-state fluorescence characteristics via external mechanical stimuli. Dyes Pigments 2018;151:140–8. https://doi.org/10.1016/j.dyepig.2017.12.053.
[10] Alterman M, Hallberg A. Fast microwave-assisted preparation of aryl and vinyl nitriles and the corresponding tetrazoles from organo-halides. J Org Chem 2000;65:7984–9. https://doi.org/10.1021/jo0009954.
[11] Powell KJ. Synthesis of alkenyl nitriles by the palladium-catalysed cyanation of vinyl halides with acetone cyanohydrin. In: Synth. Biophys. Stud. Tridachiahydropyrone Fam. Nat. Prod. Cham: Springer International Publishing; 2016. p. 105–30. https://doi.org/10.1007/978-3-319-22069-7_7.
[12] Wang XJ, Zhang SL. Cyanation of aromatic/vinylic boronic acids with α-cyanoacetates. New J Chem 2017;41:14826–30. https://doi.org/10.1039/c7nj03405a.
[13] Cao S, Liu A, Liu W, Liu X, Ren Y, Pei H, et al. Synthesis and insecticidal activity of novel thiazole acrylonitrile derivatives. J Heterocycl Chem 2017;54:3395–402. https://doi.org/10.1002/jhet.2961.
[14] Yu H, Cheng Y, Xu M, Song Y, Luo Y, Li B. Synthesis, acaricidal activity, and structure-activity relationships of pyrazolyl acrylonitrile derivatives. J Agric Food Chem 2016;64:9586–91. https://doi.org/10.1021/acs.jafc.6b04221.
[15] Hranjec M, Pavlović G, Marjanović M, Kralj M, Karminski-Zamola G. Benzimidazole derivatives related to 2,3-acrylonitriles, benzimidazo[1,2-a] quinolines and fluorenes: synthesis, antitumor evaluation in vitro and crystal structure determination. Eur J Med Chem 2010;45:2405–17. https://doi.org/10.1016/j.ejmech.2010.02.022.
[16] Briguglio I, Laurini E, Pirisi MA, Piras S, Corona P, Fermeglia M, et al. Triazolopyridinyl-acrylonitrile derivatives as antimicrotubule agents: synthesis, in vitro and in silico characterization of antiproliferative activity, inhibition of tubulin polymerization and binding thermodynamics. Eur J Med Chem 2017;141:460–72. https://doi.org/10.1016/j.ejmech.2017.09.065.
[17] Sanna P, Carta A, Gherardini L, Rahbar Nikookar ME. Synthesis and antimycobacterial activity of 3-aryl-, 3-cyclohexyl- and 3-heteroaryl-substituted-2-(1H(2H)-benzotriazol-1(2)-yl)prop-2-enenitriles, prop-2-enamides and propenoic acids. II. Farmaco 2002;57:79–87.
[18] Alam MS, Nam YJ, Lee DU. Synthesis and evaluation of (Z)-2,3-diphenylacrylonitrile analogs as anti-cancer and anti-microbial agents. Eur J Med Chem 2013;69:790–7. https://doi.org/10.1016/j.ejmech.2013.08.031.
[19] Sanna P, Carta A, Rahbar Nikookar ME. Synthesis and antitubercular activity of 3-aryl substituted-2-(1H(2H)benzotriazol-1(2)-yl)acrylonitriles. Eur J Med Chem 2000;35:535–43. https://doi.org/10.1016/S0223-5234(00)00144-6.
[20] AlNeyadi SS, Salem AA, Ghattas MA, Atatreh N, Abdou IM. Antibacterial activity and mechanism of action of the benzazole acrylonitrile-based compounds: in vitro, spectroscopic, and docking studies. Eur J Med Chem 2017;136:270–82. https://doi.org/10.1016/j.ejmech.2017.05.010.
[21] Carta A, Briguglio I, Piras S, Boatto G, La Colla P, Loddo R, et al. 3-Aryl-2-[1H-benzotriazol-1-yl]acrylonitriles: a novel class of potent tubulin inhibitors. Eur J Med Chem 2011;46:4151–67. https://doi.org/10.1016/j.ejmech.2011.06.018.
[22] Katritzky AR, Monbaliu J-CM. The chemistry of benzotriazole derivatives: a tribute to Alan Roy Katritzky, vol. 43. Liege, Belgium: Springer International Publishing Switzerland; 2016. https://doi.org/10.1007/978-3-319-31554-6.
[23] Briguglio I, Piras S, Corona P, Gavini E, Nieddu M, Boatto G, et al. Benzotriazole: an overview on its versatile biological behavior. Eur J Med Chem 2015;97:612–48. https://doi.org/10.1016/j.ejmech.2014.09.089.
[24] Jagerovic N, Jimeno ML, Alkorta I, Elguero J, Claramunt RM. An experimental (NMR) and theoretical (GIAO) study of the tautomerism of benzotriazole in solution. Tetrahedron 2002;58:9089–94. https://doi.org/10.1016/S0040-4020(02)01157-2.
[25] Ueno LT, Ribeiro RO, Rocha MS, Suárez-Iha MEV, Iha K, Machado FBC. About the benzotriazole tautomerism: an ab initio study. J Mol Struct Theochem 2003;664–665:207–15. https://doi.org/10.1016/j.theochem.2003.09.004.
[26] Pérez-Gutiérrez E, Percino MJ, Chapela VM, Cerón M, Maldonado JL, Ramos-Ortiz G. Synthesis, characterization and photophysical properties of pyridine-carbazole acrylonitrile derivatives. Materials 2011;4:562–74. https://doi.org/10.3390/ma4030562.
[27] Poddar M, Sivakumar G, Misra R. Donor-acceptor substituted 1,8-naphthalimides: design, synthesis, and structure-property relationship. J Mater Chem C 2019;7:14798–815. https://doi.org/10.1039/c9tc02634g.
[28] Wu H, Liao C, Tang H, Wang L, Meier H, Cao D. Metal-free organic dyes with di(1-benzothieno)[3,2-b:2′,3′-d]pyrrole as an auxiliary donor for efficient dye-sensitized solar cells: effect of the molecular engineering on the photovoltaic performance. Dyes Pigments 2019;171:107676. https://doi.org/10.1016/j.dyepig.2019.107676.
[29] Jadhav MM, Chowdhury TH, Bedja I, Patil D, Islam A, Sekar N. Near IR emitting novel rhodanine-3-acetic acid based two donor-π-acceptor sensitizers for DSSC: synthesis and application. Dyes Pigments 2019;165:391–9. https://doi.org/10.1016/j.dyepig.2019.02.045.
[30] Deksnys T, Simokaitiene J, Keruckas J, Volyniuk D, Bezvikonnyi O, Cherpak V, et al. Synthesis and characterisation of a carbazole-based bipolar exciplex-forming compound for efficient and color-tunable OLEDs. New J Chem 2017;41:559–68. https://doi.org/10.1039/c6nj02865a.
[31] Xing ZH, Zhuang JY, Xu XP, Ji SJ, Su WM, Cui Z. Novel oxazole-based emitters for high efficiency fluorescent OLEDs: synthesis, characterization, and optoelectronic properties. Tetrahedron 2017;73:2036–42. https://doi.org/10.1016/j.tet.2017.02.049.
[32] Wang F, Li C, Song L, Zhang X, Wang A, Zhou L, et al. A smart single molecular probe for Cu^{2+}/Fe^{3+}/Mg^{2+} by three-emission behaviors. Dyes Pigments 2019;171:107667. https://doi.org/10.1016/j.dyepig.2019.107667.
[33] Li Y, Xu K, Si Y, Yang C, Peng Q, He J, et al. An aggregation-induced emission (AIE) fluorescent chemosensor for the detection of Al(III) in aqueous solution. Dyes Pigments 2019;171:107682. https://doi.org/10.1016/j.dyepig.2019.107682.
[34] Dhoun S, Kaur I, Kaur P, Singh K. Propargylated cyanostilbene based chemodosimeter for Pd^{2+} with application in biological fluids. Dyes Pigments 2017;143:361–7. https://doi.org/10.1016/j.dyepig.2017.04.054.
[35] Dodangeh M, Gharanjig K, Tang RC, Grabchev I. Functionalization of PAMAM dendrimers with curcumin: synthesis, characterization, fluorescent improvement and application on PET polymer. Dyes Pigments 2020;174:108081. https://doi.org/10.1016/j.dyepig.2019.108081.

[36] Girgis AS, Basta AH, El-Saied H, Mohamed MA, Bedair AH, Salim AS. Synthesis, quantitative structure–property relationship study of novel fluorescence active 2-pyrazolines and application. R Soc Open Sci 2018;5:1–13. https://doi.org/10.1098/rsos.171964.
[37] Yu B, Liu D, Wang Y, Zhang T, Zhang YM, Li M, et al. A solid-state emissive and solvatofluorochromic fluorophore and its application in high-contrast, fast, and repeatable thermochromic blends. Dyes Pigments 2019;163:412–9. https://doi.org/10.1016/j.dyepig.2018.12.008.
[38] Hwang B, Engel L, Goueli SA, Zegzouti H. A homogeneous bioluminescent immunoassay to probe cellular signaling pathway regulation. Commun Biol 2020;3:1–12. https://doi.org/10.1038/s42003-019-0723-9.
[39] Moczko E, Mirkes EM, Cáceres C, Gorban AN, Piletsky S. Fluorescence-based assay as a new screening tool for toxic chemicals. Sci Rep 2016;6:1–8. https://doi.org/10.1038/srep33922.
[40] Ma H, Yang Z, Cao H, Lei L, Chang L, Ma Y, et al. One bioprobe: a fluorescent and AIE-active macromolecule; two targets: nucleolus and mitochondria with long term tracking. J Mater Chem B 2017;5:655–60. https://doi.org/10.1039/c6tb02844f.
[41] Guo Y, Zhang X, Wu F-G. A graphene oxide-based switch-on fluorescent probe for glutathione detection and cancer diagnosis. J Colloid Interface Sci 2018;530:511–20. https://doi.org/10.1016/j.jcis.2018.06.041.
[42] Hu Q, Qin C, Huang L, Wang H, Liu Q, Zeng L. Selective visualization of hypochlorite and its fluctuation in cancer cells by a mitochondria-targeting ratiometric fluorescent probe. Dyes Pigments 2018;149:253–60. https://doi.org/10.1016/j.dyepig.2017.10.002.
[43] Li H, Miao Y, Liu Z, Wu X, Piao C, Zhou X. A mitochondria-targeted fluorescent probe for fast detecting hypochlorite in living cells. Dyes Pigments 2020;176:108192. https://doi.org/10.1016/j.dyepig.2020.108192.
[44] Jantra S, Butta P, Jithavech P, Rojsitthisak P, Palaga T, Rashatasakhon P, et al. "Turn on" orange fluorescent probe based on styryl-BODIPY for detection of hypochlorite and its application in live cell imaging. Dyes Pigments 2019;162:189–95. https://doi.org/10.1016/j.dyepig.2018.10.007.
[45] Wang X, Shao J, Hu Y. An efficient chemodosimeter for Cu(II) ions based on hydrolysis of fluorescein and its utility in live cell imaging. Dyes Pigments 2019;5:655–60. https://doi.org/10.1016/j.dyepig.2019.107680.
[46] Palion-Gazda J, Machura B, Klemens T, Szlapa-Kula A, Krompiec S, Siwy M, et al. Structure-dependent and environment-responsive optical properties of the trisheterocyclic systems with electron donating amino groups. Dyes Pigments 2019;166:283–300. https://doi.org/10.1016/j.dyepig.2019.03.035.
[47] Chan-Navarro R, Jiménez-Pérez VM, Muñoz-Flores BM, Dias HVR, Moggio I, Arias E, et al. Luminescent organoboron compounds derived from salicylidenebenzohydrazide: synthesis, characterization, structure, and photophysical properties. Dyes Pigments 2013;99:1036–43. https://doi.org/10.1016/j.dyepig.2013.07.039.
[48] Chua MH, Zhou H, Lin TT, Wu J, Xu J. Triphenylethylenyl-based donor-acceptor-donor molecules: studies on structural and optical properties and AIE properties for cyanide detection. J Mater Chem C 2017;5:12194–203. https://doi.org/10.1039/c7tc04400c.
[49] Lakowicz JR. Principles of fluorescence spectroscopy. second ed. New York: Kluwer Academic/Plenum Publishers; 1999. https://doi.org/10.1007/978-0-387-46312-4.
[50] Corona-López MM, Jiménez Pérez VM, Chan-Navarro R, Ibarra-Rodríguez M, Dias HVR, Chávez-Reyes A, et al. Synthesis, characterization, photophysical properties of new fluorescent boron Schiff bases (BOSCHIBAs) and their application as cytoplasm staining dyes in vitro. J Organomet Chem 2017;852:64–73. https://doi.org/10.1016/j.jorganchem.2017.10.003.
[51] Xue P, Zhang C, Wang K, Liang M, Zhang T. Alkyl chain-dependent cyano-stilbene derivative's molecular stacking, emission enhancement and fluorescent response to the mechanical force and thermal stimulus. Dyes Pigments 2019;163:516–24. https://doi.org/10.1016/j.dyepig.2018.12.036.
[52] Indapurkar A, Henriksen B, Tolman J, Fletcher J. Evaluation of triazole-chelated lanthanides as chemically stabile bioimaging agents. J Pharm Sci 2013;102:2589–98. https://doi.org/10.1002/jps.23616.
[53] Kucherak OA, Didier P, Mély Y, Klymchenko AS. Fluorene analogues of prodan with superior fluorescence brightness and solvatochromism. J Phys Chem Lett 2010;1:616–20. https://doi.org/10.1021/jz9003685.
[54] Wang L, Xia Q, Hou M, Yan C, Xu Y, Qu J, et al. A photostable cationic fluorophore for long-term bioimaging. J Mater Chem B 2017;5:9183–8. https://doi.org/10.1039/c7tb02668d.
[55] Zhang W, Zhao X, Gu W, Cheng T, Wang B, Jiang Y, et al. A novel naphthalene-based fluorescent probe for highly selective detection of cysteine with a large Stokes shift and its application in bioimaging. New J Chem 2018;42:18109–16. https://doi.org/10.1039/c8nj04425b.
[56] Lampidis TJ, Castello C, Del Giglio A, Pressman BC, Viallet P, Trevorrow KW, et al. Relevance of the chemical charge of rhodamine dyes to multiple drug resistance. Biochem Pharmacol 1989;38:4267–71. https://doi.org/10.1016/0006-2952(89)90525-X.
[57] Kim K, Lee M, Park H, Kim JH, Kim S, Chung H, et al. Cell-permeable and biocompatible polymeric nanoparticles for apoptosis imaging. J Am Chem Soc 2006;128:3490–1. https://doi.org/10.1021/ja057712f.
[58] Ortega-Villarreal AS, Hernández-Fernández E, Jensen C, Valdivia-Berroeta GA, Garrard S, López I, et al. Synthesis and characterization of ethyl benzotriazolyl acrylate-based D-π-A fluorophores for live cell-based imaging applications. RSC Adv 2019;9:8759–67. https://doi.org/10.1039/c9ra00108e.
[59] Herzog V, Farquhar MG. Luminal membrane retrieved after exocytosis reaches most Golgi cisternae in secretory cells. Proc Natl Acad Sci 1977;74:5073–7. https://doi.org/10.1073/pnas.74.11.5073.
[60] Berlin RD, Oliver JM. Surface functions during mitosis. II. Quantitation of pinocytosis and kinetic characterization of the mitotic cycle with a new fluorescence technique. J Cell Biol 1980;85:660–71. https://doi.org/10.1083/jcb.85.3.660.
[61] Gruenberg J, Griffiths G, Howell KE. Characterization of the early endosome and putative endocytic carrier vesicles in vivo and with an assay of vesicle fusion in vitro. J Cell Biol 1989;108:1301–16. https://doi.org/10.1083/jcb.108.4.1301.
[62] Herman B. Absorption and emission maxima for common fluorophores. Curr Protoc Cell Biol 2001:A.1E.1–5. https://doi.org/10.1109/TIM.2012.2218681.
[63] Zhang J, Wu W, Ji X, Cao S. Perfluorobutyl iodide-assisted direct cyanomethylation of azoles and phenols with acetonitrile. RSC Adv 2015;5:20562–5. https://doi.org/10.1039/c5ra02242h.
[64] Sheldrick GM. SAINT (version 6.02), SADABS (version 2.03). Madison, WI: Bruker AXS Inc.; 2002.
[65] Sheldrick GM. SADABS, program for empirical absorption correction of area detector data. 1996.
[66] Sheldrick GM. SHELXT-integrated space-group and crystal-structure determination. Acta Crystallogr Sect A Found Adv 2015;A71:3–8. https://doi.org/10.1107/S2053273314026370.
[67] Sheldrick GM. Crystal structure refinement with SHELXL. Acta Crystallogr Sect C Struct Chem 2015;C71:3–8. https://doi.org/10.1107/S2053229614024218.
[68] Felouat A, D'Aléo A, Fages F. Synthesis and photophysical properties of difluoroboron complexes of curcuminoid derivatives bearing different terminal aromatic units and a meso-aryl ring. J Org Chem 2013;78:4446–55. https://doi.org/10.1021/jo400389h.
[69] Williams ATR, Winfield SA, Miller JN. Relative fluorescence quantum yields using a computer-controlled luminescence spectrometer. Analyst 1983;108:1067–71. https://doi.org/10.1039/an9830801067.